Absolute density of precursor SiH_3 radicals and H atoms in H_2-diluted SiH_4 gas plasma for deposition of microcrystalline silicon films

Yusuke Abe, Kenji Ishikawa, Keigo Takeda, Takayoshi Tsutsumi, Atsushi Fukushima, Hiroki Kondo, Makoto Sekine, and Masaru Hori

Citation: Appl. Phys. Lett. **110**, 043902 (2017); doi: 10.1063/1.4974821
View online: http://dx.doi.org/10.1063/1.4974821
View Table of Contents: http://aip.scitation.org/toc/apl/110/4
Published by the American Institute of Physics

Absolute density of precursor SiH_3 radicals and H atoms in H_2-diluted SiH_4 gas plasma for deposition of microcrystalline silicon films

Yusuke Abe, Kenji Ishikawa,[a] Keigo Takeda, Takayoshi Tsutsumi, Atsushi Fukushima, Hiroki Kondo, Makoto Sekine, and Masaru Hori
Nagoya University, Nagoya 463-8603, Japan

(Received 16 November 2016; accepted 11 January 2017; published online 23 January 2017)

Microcrystalline hydrogenated silicon films were produced at a high deposition rate of about 2 nm/s by using a capacitively coupled plasma under a practical pressure of around 1 kPa. The SiH_4 source gas was almost fully dissociated when highly diluted with H_2 gas, and the dominant species in the gas phase were found to be SiH_3 radicals, which are film-growth precursors, and H atoms. The absolute density of these species was measured as the partial pressure of SiH_4 gas was varied. With the increasing SiH_4 gas flow rate, the SiH_3 radical density, which was on the order of $10^{12}\,cm^{-3}$, increased linearly, while the H-atom density remained constant at about $10^{12}\,cm^{-3}$. The film growth mechanism was described in terms of precursors, based on the measured flux of SiH_3 radicals and H atoms, and the relative fraction of higher-order radicals. *Published by AIP Publishing.*
[http://dx.doi.org/10.1063/1.4974821]

Microcrystalline hydrogenated silicon (μc-Si:H) is a promising material for use in thin films in the bottom cell of tandem solar cells. Such films are currently widely fabricated using plasma-enhanced chemical vapor deposition (PECVD).[1] Since μc-Si:H exhibits lower optical absorption of the visible solar spectrum than hydrogenated amorphous silicon (a-Si:H), the μc-Si:H films with a thickness of more than 2 μm are required for solar cell applications. Therefore, a practical technique that is capable of producing films at a high deposition rate of around 2 nm/s is strongly required for the low-cost production of thin-film tandem solar cells.[2–4]

In PECVD, chemical species such as monosilane radicals (SiH_m), polysilane radicals ($Si_{n\geq 2}H_m$), positive ions ($Si_nH^+{}_m$), and Si nanoparticles are generated by electron-collision effects such as dissociation and ionization of SiH_4 molecules.[5,6] Similar to the case for a-Si:H films, the SiH_3 radicals are known to be the dominant deposition precursors during the growth of μc-Si:H films.[7,8] To grow μc-Si:H films, a large amount of H atoms is commonly supplied to the growth surface because this improves the crystallinity of the thin Si films.[6] This is thought to be because H atoms fully cover the Si surface and then recombine to form the hydrogen molecules. These recombination reactions cause local heating of the surface.[6] The H coverage enhances the diffusion of SiH_3 radicals on the surface, and Si–Si bonds are formed by adsorption at dangling bond sites. Moreover, H atoms reaching the growth surface preferentially break the weak Si–Si bonds that form an amorphous network, leading to a removal of weakly bonded Si atoms. These sites then absorb SiH_3, thus creating rigid strong Si–Si bonds, giving rise to an ordered structure.[6] Film crystallinity can also be improved by the etching of weakly bonded amorphous phases by H atoms. A network of Si–Si bonds is reconstructed by the removal of subsurface amorphous phases in H-rich regions.[9–11] However, to understand the growth mechanism for μc-Si:H films at higher deposition rates and practical pressures of around 1 kPa, it is necessary to measure the absolute density of H atoms and SiH_3 radicals under such higher pressures. No such study has yet been undertaken for deposition conditions that can yield a growth rate of around 2 nm/s.

In the present study, using cavity ring-down spectroscopy (CRDS) and vacuum ultraviolet laser absorption spectroscopy (VUVLAS),[12,13] the absolute density of SiH_3 radicals and H atoms was measured under conditions that produced μc-Si:H films at a growth rate of approximately 1.8 nm/s. The films were grown using a capacitively coupled plasma excited by a very high frequency (VHF) of 60 MHz. The relative fractions of higher-order radicals were measured using the quadrupole mass spectroscopy (QMS).

The plasma discharge was sustained by supplying a VHF power of 400 W to the upper electrode, while the lower electrode was grounded. The gap between the electrodes was 10 mm. The radius of the discharge region was 65 mm, and the discharge volume was 132.7 cm^3. The gas mixture ratios of SiH_4 to H_2 gases were varied from 7 to 15 sccm, while H_2 gas at a fixed flow rate of 470 sccm was introduced using a showerhead upper electrode. A total pressure of 1.2 kPa (9 Torr) was maintained by controlling the conductance of the vacuum-pump tubing.

The desired Raman crystallinity factor of 0.6 for the application of μc-Si:H films to solar cell devices[14] was obtained at a deposition rate of 1.8 nm/s and an SiH_4 gas flow rate of 11 sccm. The deposition rates increased with increasing the SiH_4 flow rates; however, the Raman crystallinity depended strongly on the surface reactions with respect to the precursors of H atom and SiH_3 radical fluxes ratio.[4] Therefore, the typical experiment was conducted under the condition as identical as the previous report.[4,12,13] The details of the film deposition procedure and the film properties have previously been reported.[4,12,13] The VUVLAS system for measuring the H-atom density and the results obtained have also been described elsewhere.[12]

The CRDS setup consisted of an optical cavity with a length of 170 cm between two high-reflectivity plano-concave

[a]Electronic mail: ishikawa.kenji@nagoya-u.jp

mirrors (LASEROPTIK GMBH). Two sets of mirrors with a reflectivity of 99.2% and a narrow bandwidth at 220 nm and 280 nm were used. Laser light with a wavelength of 220 nm is absorbed by SiH_3 radicals. However, light scattering by the Si nanoparticles should also be taken into account during the discharge period following plasma ignition. Since such scattering is prominent at about 280 nm, the cavity loss was simultaneously measured at both 220 and 280 nm.[15] The light source was an optical parametric oscillator (OPO; Spectra-Physics FLEXI-AT-DW) pumped using the frequency-tripled output of an Nd:YAG laser (Spectra-Physics PRO-250T-A3W). The pulse duration was 8 ns and the repetition rate was 10 Hz. Highly reflective optics was used to guide the light and introduce it into the optical cavity. Light leaking from the back of the cavity mirror was detected through a bandpass filter using a photomultiplier tube (Hamamatsu, R928). The cavity ring-down signals were recorded using a digital oscilloscope (Tektronix DPO4000 series) using a trigger signal from a delay generator (Stanford Research Systems SR535) to tune the delay time against the laser pulse and the plasma ignition times. The cavity mirrors were blown with H_2 gas at a flow rate of 30 sccm in order to prevent any film deposition.

In CRDS, the light intensity leaking from the cavity is represented by

$$I_t = I_0 \exp\left(-\frac{t}{\tau_r}\right), \tag{1}$$

where τ_r is the ring-down time given by

$$\tau_r = \frac{l/c}{L_{tot}} = \frac{l/c}{L_0 + L_{abs} + L_{sca}}, \tag{2}$$

where l is the cavity length and c is the velocity of light. The total cavity loss, L_{tot}, is given by the sum of the primary cavity loss L_0, the cavity loss L_{abs} due to light absorption by species in the cavity, and the cavity loss L_{sca} due to light scattering by species in the cavity. When no such absorption or scattering occurs in the course of multiple trips between the cavity mirrors, τ_r is simply determined by L_0, which is related to the effective transmittance $(1-R)$ by

$$L_0 = 1 - R, \tag{3}$$

where R is the reflectivity of the mirrors. When absorption or scattering due to multiple species takes place, the absorption loss $L_{abs,i}$ due to the ith species is given by

$$L_{abs} = k_i(\nu) d_{abs,i} = N_{abs,i}\sigma_{abs,i}(\nu) d_{abs,i}, \tag{4}$$

and the scattering loss $L_{sca,i}$ due to the ith species is

$$L_{sca} = N_{sca,i}\sigma_{sca,i} d_{sca,i}, \tag{5}$$

where $N_{abs,i}$ and $N_{sca,i}$ are the densities of the absorbing and scattering species, respectively, and $\sigma_{abs,i}(\nu)$ and $\sigma_{sca,i}$ are the corresponding light absorption and scattering cross sections. Therefore, the cavity losses due to absorption and scattering by all species is given by

$$L_{tot} - L_0 = \sum_i L_{abs,i} + \sum_i L_{sca,i}. \tag{6}$$

A quadrupole mass spectrometer (Hiden Analytical Ltd., EQP) was used to analyze the residual gas. The orifice diameter was approximately 0.1 mm and a two-stage pumping system produced an ultrahigh vacuum ($<10^{-4}$ Pa). The electron energy for ionization was 70 eV and the emission current was 30 μA.

Figure 1(a) shows typical cavity-ring-down signals as a function of elapsed time from laser-pulse input into the optical cavity, measured in the absence and presence of a plasma. In both cases, the decay is exponential but is clearly faster in the presence of the plasma, indicating absorption and scattering by species in the cavity during multiple trips between the mirrors.

Figure 1(b) shows the temporal evolution of the cavity loss determined from the decay curves at wavelengths of 220 and 280 nm, measured just after plasma ignition. Immediately following plasma ignition, the cavity loss at 220 nm remains a constant. This loss is associated with absorption by the SiH_3 radicals, whose density became stable during the initial period of approximately 3 ms. In contrast, the cavity loss at 280 nm mainly due to scattering by the Si nanoparticles increases sharply after the first 3 ms. Taking into account the detection limit for the ring-down time and the standard deviation of data accumulated over 1000 laser shots, it was determined that the

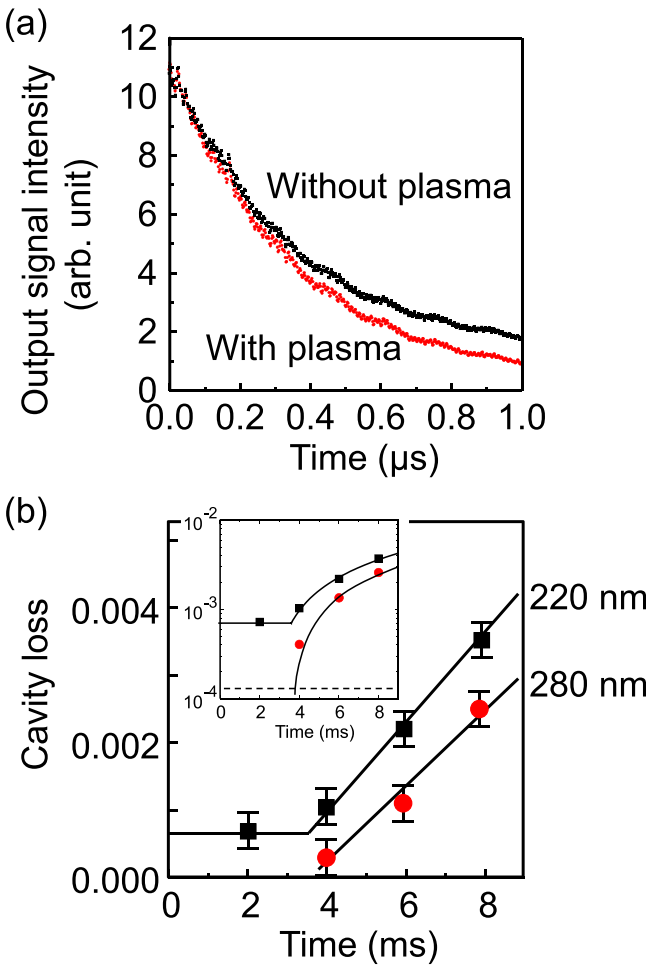

FIG. 1. (a) Typical CRDS cavity decay profiles with and without plasma. (b) Time-evolution of cavity loss after plasma ignition at wavelengths of 220 and 280 nm. The lines are guides for the eye. Inset figure shows a logarithmic plot. The dashed line is a limit of detection.

absorption signal within 3 ms was attributed to the formation of SiH_3 radicals after plasma ignition, and this was used to measure their absolute density.

Based on the above results, we now consider the formation mechanism for the Si nanoparticles. The experiments in the present study were performed at a pressure of 1.2 kPa. This is about one order of magnitude higher than the value of 133 Pa used in a previous study, where measurements were carried out over a period of a few seconds.[15] The cavity losses measured at 280 nm in the present study were about three orders of magnitude lower than those in the previous study. Nanoparticle growth is thought to occur by the reactions

$$SiH_4 + e \rightarrow SiH_2 + H_2,\ SiH_4 + SiH_2 \rightarrow Si_2H_6,$$
$$Si_2H_6 + SiH_2 \rightarrow Si_3H_8, \cdots\cdots \quad (7)$$

and the growth rate depends on the density of the parent SiH_4 molecules. This involves reactions between short-lifetime species such as $SiH_{x\leq 2}$ and SiH_4. The nanoparticle growth is hypothetically represented as a series of chain reactions: $n=1$, $[SiH_4]$; $n=2$, $[Si_2H_6]=[SiH_4][SiH_2]=[SiH_4]\ r_2\ n_e\ [SiH_4]=r_2\ n_e\ [SiH_4]^2$; $n=3$, $Si_3H_9=[Si_2H_6]\ r_3\ n_e^2\ [SiH_4]^3 = r_3\ n_e^2\ [SiH_4]^3$; …, where the angle brackets represent concentration. The r's are a rate coefficient for each electron-collision induced reaction. The density of nanoparticles, $N(Si_nH_{2n+2})$, can be expressed in the form of a rate equation as

$$\frac{dN(Si_nH_{2n+2})}{dt} = A[n_e]^{n-1}[N(SiH_4)]^n - L, \quad (8)$$

where L is the loss rate for nanoparticles, n_e is the plasma density, and the A is an overall reaction rate constant that includes the generation of $SiH_{x\leq 2}$ and reactions between $SiH_{x\leq 2}$ and Si_mH_{2m+2} ($m \geq 1$), i.e., $A = \Pi\ r_n$. In Eq. (8), the generation rate for nanoparticles depends strongly on n_e and the SiH_4 density, $N(SiH_4)$, both of which increase with pressure. This explains why the particle growth rate at 1.2 kPa is three orders of magnitude higher than that at 133 Pa.

Figure 2(a) shows the density of SiH_3 radicals as a function of the SiH_4 flow rate. For reference, the H-atom density obtained in a previous study is also plotted.[12] It can be seen that the density of SiH_3 radical increases linearly with the increasing flow rate. The SiH_3 radicals are generated by the dissociation of SiH_4 under the influence of electron impact. Since the density of H atoms was constant, scavenging of H atoms from SiH_4 based on the following reaction can be considered to be negligible:[16]

$$SiH_4 + H \rightarrow SiH_3 + H_2. \quad (9)$$

The H-atom density is determined by the following rate equations for the dominant reactions:

$$\frac{dN(H_2)}{dt} = \Phi_{H_2} + k_3 N(H) N(SiH_4) - (2k_1 n_e + 1/\tau_{pump}) N(H_2), \quad (10)$$

$$\frac{dN(SiH_4)}{dt} = \Phi_{SiH_4} - (k_2 n_e + k_3 N(H) + 1/\tau_{pump}) N(SiH_4), \quad (11)$$

$$\frac{dN(H)}{dt} = k_1 n_e N(H_2) + k_2 n_e N(SiH_4) - (k_3 N(SiH_4) + 1/\tau_d) N(H), \quad (12)$$

where Φ_x is the flow rate per unit volume for molecule x, k_x ($x = 1$–3) is the rate constant for each reaction, $N(x)$ is the density of species x, τ_{pump} is the pumping loss decay time, and τ_d is the diffusion lifetime for H atoms. In the present study, the values of τ_{pump} and τ_d were estimated to be 61 ms and 0.15 ms, respectively, based on the chamber geometry and the probability of surface loss of an H atom (approximately 1).[4] The unknown parameters $k_1 n_e$ and $k_2 n_e$ were estimated from the results of optical emission measurements using a trace amount of Xe gas. The threshold energy for Xe emission at 823.1 nm is 9.82 eV, which is similar to the electron-impact dissociation threshold for SiH_4 (8.75 eV) and H_2 (8.8 eV). Therefore, the values for $k_1 n_e$ and $k_2 n_e$ can be estimated based on the Xe emission intensity.[17] Figure 3 shows the dependence of the Xe emission intensity on the SiH_4 flow rate. Since the intensity appears to be independent of the flow rate, it can be concluded that $k_1 n_e$ and $k_2 n_e$ are constant for the experimental conditions used in the present study.

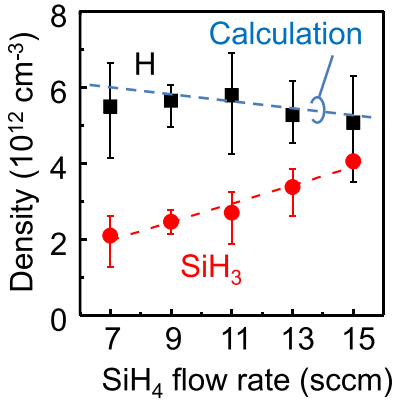

FIG. 2. SiH_3 density as a function of SiH_4 flow rate. The dashed lines through the data are a guide for the eye. For reference, the H-atom density in Fig. 2 of Ref. 12 is also reproduced here. The dashed line shows the calculated H-atom density.

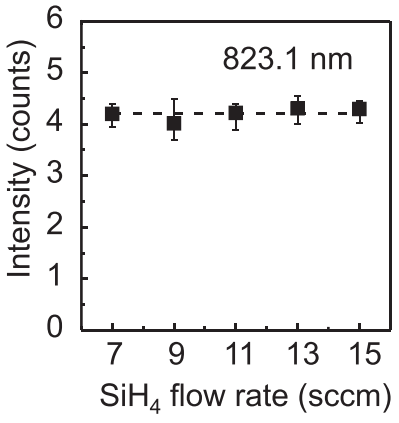

FIG. 3. Optical emission intensity at 823.1 nm as a function of SiH_4 flow rate. The dashed line is a guide for the eye.

The calculated H-atom density as a function of the SiH_4 flow rate is plotted as a dotted line in Fig. 2. The calculation was carried out by assuming an electron density of $10^{10}\,cm^{-3}$, an electron temperature of 1.5 eV, and a gas temperature of 473 K, and using the estimated rate constants of $1.7 \times 10^{-11}\,cm^{-6}\,s^{-1}$ for k_1, $4.2 \times 10^{-10}\,cm^{-6}\,s^{-1}$ for k_2, and $2.0 \times 10^{-12}\,cm^{-6}\,s^{-1}$ for k_3.[5,18,19] It can be seen that there is a good agreement between the calculated H-atom density and the measured values. This is consistent with H scavenging from SiH_4 to produce SiH_3 radicals being negligible under these conditions. The loss term $k_3N(SiH_4)N(H)$ and the generation term $k_2 n_e N(SiH_4)$ in Eq. (12) were both estimated to be about 10^{15}. Thus, the loss of H atoms with SiH_4 is balanced by the generation of H atoms from SiH_4 by electron impact.

The flux of SiH_3 radicals at the surface was calculated by assuming a sticking probability of 0.09[20] and a temperature of 473 K, using the following equation:

$$\Gamma_{SiH_3} = \frac{s}{4} n_{SiH_3} \sqrt{\frac{8k_B T_{SiH_3}}{\pi m}}, \tag{13}$$

where s is the sticking probability for SiH_3. Under identical conditions, we measured the film thickness. From the deposition rate, R_d, the flux of deposited precursors, Γ_P, can be estimated using

$$\Gamma_P = \frac{R_d \rho}{m_{Si}}, \tag{14}$$

where ρ is the film density ($2.18\,g\,cm^{-3}$),[21] and m_{Si} is the atomic mass of Si (4.69×10^{-23} g). By comparing the fluxes Γ_{SiH_3} and Γ_P, the contribution of the precursors to film growth was analyzed. The results indicated that SiH_3 radicals constituted 45% of the deposition precursors. The flux of SiH_3 radicals can then be more accurately rewritten to include the surface loss probability, α, as

$$\Gamma_{SiH_3} = \frac{1}{4} \frac{s}{1-\alpha} n^{(s)}_{SiH_3} \sqrt{\frac{8k_B T_{SiH_3}}{\pi m}}, \tag{15}$$

where $n^{(s)}_{SiH_3}$ is the density of SiH_3 radicals at the substrate surface. Experimentally, $n^{(s)}_{SiH_3}$ can be estimated based on the spatial distribution of SiH_3 radicals; however, we could not determine more accurate values for $n^{(s)}_{SiH_3}$. Here, we use the notation of $n^{(s)}_{SiH_3}$ for the SiH_3 density at the substrate surface. On the other hand, the surface-loss flux Γ_{SiH_3} in Eq. (13) is obtained based on a surface loss probability of 0.5 for the SiH_3 radicals reported for μc-Si:H growth at a substrate temperature of around 200 °C.[6] The SiH_3 radical contribution to film growth is 59% based on Eq. (15), which is 1.3 times higher than the value of 45% based on Eq. (13), since $n^{(s)}_{SiH_3}$ is smaller than n_{SiH_3}. Beyond the discrepancy, it will be necessary to determine more accurate values of the SiH_3 radical density at the vicinity of the surface and investigate the dependence of the surface loss probability on the surface temperature.

Finally, other types of film-growth precursors were investigated. Figure 4(a) shows a quadrupole mass spectrum of an H_2/SiH_4 plasma produced under the same discharge conditions used in this study. The SiH_4 flow rate was 17 sccm. The spectrum indicates that in addition to monosilane, higher-order silanes (Si_nH_x; $n > 1$) are also present. Under these experimental conditions, although nanoparticle formation can be eliminated, the production of higher-order radicals cannot be neglected at the relatively high pressure of 1.2 kPa. As shown in Fig. 4(b), the signal intensity for SiH_x and higher-order radicals such as Si_2H_x, Si_3H_x, and Si_4H_x increased roughly linearly with increasing SiH_4 flow rate, so that the relative fraction of these radicals remained constant. Since a similar relationship was found for SiH_3 radicals, it can be concluded that these radicals are the main (50% or more) film-deposition precursors. The contribution of higher-order radicals ($Si_{n\geq 2}H_m$) is also larger at pressures of around 1 kPa than at lower pressures. It is therefore extremely important to determine the absolute density of SiH_3 radicals and H atoms in order to clarify the reaction mechanisms during μc-Si:H thin film formation in a highly H_2-diluted SiH_4 plasma. This information is also expected to be important in a wide range of other PECVD fields.

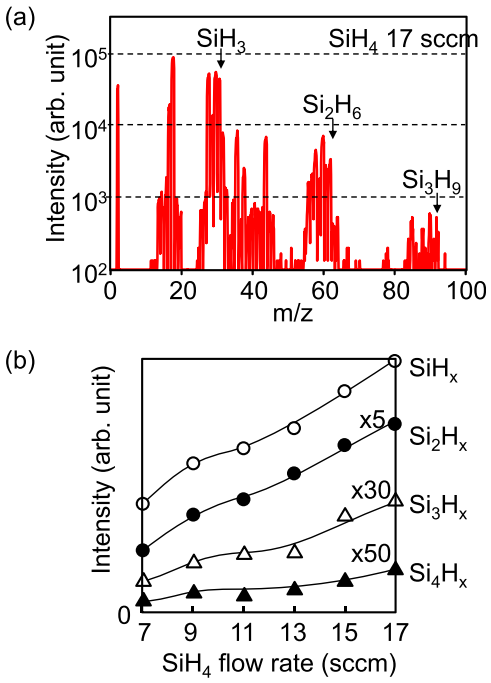

FIG. 4. (a) Quadruple mass spectrogram for plasma of H_2-diluted SiH_4 for a flow rate of 17 sccm. (b) Dependence of mass spectral intensity for higher-order Si_nH_x (n = 1,2,3,4) radicals on SiH_4 flow rate.

The authors would like to thank Dr. S. Nunomura of AIST Tsukuba for fruitful discussions and K. Kojima, K. Miwa, and L. Ya for their support with the experiments.

[1]H. Keppner, J. Meier, P. Torres, D. Fischer, and A. Shah, Appl. Phys. A **69**, 169 (1999).
[2]M. Fukawa, S. Suzuki, L. Guo, M. Kondo, and A. Matsuda, Sol. Energy Mater. Sol. Cells **66**, 217 (2001).
[3]U. Graf, J. Meier, U. Kroll, J. Bailat, C. Droz, E. Vallat-Sauvain, and A. Shah, Thin Solid Films **427**, 37 (2003).
[4]Y. Abe, S. Kawashima, A. Fukushima, Y. Lu, K. Takeda, H. Kondo, K. Ishikawa, M. Sekine, and M. Hori, J. Appl. Phys. **113**, 033304 (2013).
[5]J. Perrin, O. Leroy, and M. C. Bordage, Contrib. Plasma Phys. **36**, 3 (1996).

[6]A. Matsuda, J. Non-Cryst. Solids **338–340**, 1 (2004).
[7]N. Itabashi, N. Nishiwaki, M. Magane, S. Naito, T. Goto, A. Matsuda, C. Yamada, and E. Hirota, Jpn. J. Appl. Phys. **29**, L505 (1990).
[8]T. Nagai, A. H. M. Smets, and M. Kondo, Jpn. J. Appl. Phys. **45**, 8095–8098 (2006).
[9]C. C. Tsai, G. B. Anderson, R. Thompson, and B. Wacker, J. Non-Cryst. Solids **114**, 151 (1989).
[10]F. Kaïl, A. Fontcuberta, I. Morral, A. Hadjadj, P. Roca I Cabarrocas, and A. Beorchia, Philos. Mag. **84**, 595 (2004).
[11]K. Nakamura, K. Yoshino, S. Takeoka, and I. Shimizu, Jpn. J. Appl. Phys. **34**, 442 (1995).
[12]Y. Abe, A. Fukushima, K. Takeda, H. Kondo, K. Ishikawa, M. Sekine, and M. Hori, Appl. Phys. Lett. **101**, 172109 (2012).
[13]Y. Abe, A. Fukushima, K. Takeda, H. Kondo, K. Ishikawa, M. Sekine, and M. Hori, J. Appl. Phys. **113**, 013303 (2013).
[14]S. Nunomura and M. Kondo, J. Phys. D **42**, 185210 (2009).
[15]T. Nagai, A. H. M. Smets, and M. Kondo, Jpn. J. Appl. Phys. **47**, 7032 (2008).
[16]M. Kondo, M. Fukawa, L. Guo, and A. Matsuda, J. Non-Cryst. Solids **266–269**, 84 (2000).
[17]S. Takashima, M. Hori, T. Goto, and K. Yoneda, J. Appl. Phys. **89**, 4727 (2001).
[18]S. J. B. Corrigan, J. Chem. Phys. **43**, 4381 (1965).
[19]E. Meeks, J. Vac. Sci. Technol., A **16**, 544 (1998).
[20]A. Matsuda, K. Nomoto, Y. Takeuchi, A. Suzuki, A. Yuuki, and J. Perrin, Surf. Sci. **227**, 50 (1990).
[21]B. Strahm, A. A. Howling, L. Sansonnens, and C. Hollenstein, Plasma Sources Sci. Technol. **16**, 80 (2007).